Chemical Engineering Journal 519 (2025) 165032

Contents lists available at ScienceDirect

Chemical Engineering Journal

journal homepage: www.elsevier.com/locate/cej

Surface-engineered silica particles for highly selective organic gas sensors

In Hwa Ko [a], So Jeong Park [a], Yeong Don Park [a,b,*]

[a] Department of Energy and Chemical Engineering, Incheon National University, Incheon 22012, Republic of Korea
[b] Innovation Center for Chemical Engineering, Incheon National University, Incheon 22012, Republic of Korea

ARTICLE INFO

Keywords:
P3HT
Silica
Organic gas sensor
SAM
OFET

ABSTRACT

Creating gas sensors with excellent selectivity and sensitivity is essential for applications in air quality control and workplace hazard detection. In this study, we explored the effects of surface-functionalized silica particles on the performance of organic field-effect transistor (OFET) based gas sensors using poly(3-hexylthiophene) (P3HT) as the active layer. Silica particles were modified with self-assembled monolayers (SAMs), including methyl (C), ethylenediamine (2 N), diethylenetriamine (3 N), and thiol (S) groups as well as the bare hydroxyl (O) group, to enhance gas adsorption. The gas sensing performance was evaluated for nitrogen dioxide (NO_2), sulfur dioxide (SO_2), and carbon dioxide (CO_2). The 3 N-silica demonstrated the highest sensitivity to NO_2 due to strong amine-gas interactions. In contrast, for SO_2, the S-silica exhibited the highest sensing performance due to the strong chemical interaction between SO_2 and the thiol groups. Additionally, air stability tests revealed that functionalized silica enhances the long-term stability of OFET devices, with 3 N- and O-silica achieving the highest recovery rates because of the strong adsorption of H_2O. These findings provide a crucial direction for advancing next generation organic electronic devices by addressing the challenges of low sensitivity and stability in organic gas sensors.

1. Introduction

The development of high-performance gas sensors is essential for a wide range of applications, including environmental monitoring, industrial safety, and public health [1–5]. Among the various materials used in gas sensors, conjugated polymers have garnered significant attention because of their flexibility, low-cost fabrication, and tunability through chemical structure tailoring [6–12]. In particular, p-type conjugated polymers have shown promise for portable gas-sensing applications owing to their flexibility, lightness, and sensitivity to electron-withdrawing oxidative gases, such as nitrogen dioxide (NO_2) and sulfur dioxide (SO_2) [13].

Nonetheless, the inherent drawbacks of conjugated polymers, including limited sensitivity and inadequate selectivity, have led to increasing interest in hybrid systems that integrate these materials with functional additives to enhance performance [14–18]. A promising approach involves the incorporation of surface-functionalized particles into the active polymer layer.

Self-assembled monolayers (SAMs) have been widely employed to modify the surface properties of oxide layers, enabling precise control over the surface functional groups [19,20]. By grafting various SAMs onto the silica surface, functional groups such as alkyl, amine, and thiol can be introduced, with each interacting selectively with the gas molecules [21,22]. These functional groups can significantly influence gas sensing performance by altering the charge carrier density and interaction strength between the gas molecules and sensing material.

In this study, we explored the effects of surface-functionalized silica particles on the performance of an organic field-effect transistor (OFET) based gas sensor. We aimed to enhance the sensitivity and selectivity of the sensor toward harmful gases by introducing various SAMs with functional groups on the silica surface. Poly(3-hexylthiophene) (P3HT) is one of the most widely studied p-type semiconducting polymers. Its conjugated backbone ensures efficient charge transport, while the alkyl side chains enhance solubility and enable the cost-effective fabrication of uniform thin films via solution processing. Moreover, p-type nature of P3HT makes it highly responsive to oxidizing gases such as NO_2 and SO_2, which induce a p-doping effect and significantly increase the drain current. These advantages make P3HT a suitable choice as the active material in this study.

The incorporation of silica particles into the P3HT active matrix is expected to further enhance sensing performance by increasing the adsorption of gas molecules. By thoroughly examining sensor responses,

---

* Corresponding author at: Department of Energy and Chemical Engineering, Incheon National University, Incheon 22012, Republic of Korea.
E-mail address: ydpark@inu.ac.kr (Y.D. Park).

https://doi.org/10.1016/j.cej.2025.165032
Received 27 March 2025; Received in revised form 25 May 2025; Accepted 16 June 2025

recovery behavior, and sensitivity levels, this study highlights the capability of hybrid materials to serve as effective platforms for next-generation organic gas sensing technologies. In this study, we propose a practical method using SAM-treated silica particles. In contrast to previous approaches involving complex ligand exchange for the modification of porous materials such as metal-organic frameworks or covalent organic frameworks, our method provides simple and commercially available SAM chemistry for surface functionalization.

2. Experimental details

2.1. Surface modification and characterization of silica particle

The silica particle used in this study was prepared by modifying the surface of various silane coupling agents purchased from Sigma-Aldrich. The silica particle was surface-treated by vapor deposition and thinly spread in a round-bottomed flask before further treatment with ozone for 40 min to form hydroxyl groups (-OH, O) [23]. Subsequently, the hydroxylated silica particle was placed in a vacuum chamber along with the silane coupling agents and left in a vacuum oven for 12 h. Four different silane coupling agents were used in this experiment: trichloro(octyl)silane (C), N-[3-(trimethoxysilyl)propyl]ethylenediamine (2 N), N-[3-(trimethoxysilyl)propyl]ethylenediamine (3 N), and (3-mercaptopropyl)trimethoxysilane (S). The silica particle was then baked in an oven at 125 °C for an hour (Fig. S1).

The specific surface areas of the silica particles were measured using the Brunauer–Emmett–Teller (BET) model over a consistent linear range [24]. X-ray photoelectron spectroscopy (XPS, PHI 5000 Versa Probe II) equipped with an Al Kα radiation source (photon energy = 1486.6 eV) was employed to investigate the surface functional groups of the functionalized silica particle.

2.2. Fabrication of organic gas sensor

The P3HT employed in this work was obtained from Rieke Metals and possesses a molecular weight of 58 kDa with a regioregularity of 95%. A heavily doped n-type silicon wafer coated with a 300 nm-thick silicon dioxide layer was employed as the substrate. The substrates underwent sequential ultrasonic cleaning in acetone and ethanol, each for 30 min. Following the cleaning process, the substrates were treated with UV-ozone for 40 min to enhance surface activation and subsequently modified by spin-coating a layer of hexamethyldisilazane (HMDS) at a speed of 2500 rpm for 30 s. The surface-treated Si substrate was baked in a vacuum oven at 125 °C for an hour.

The polymer composite was prepared by dissolving P3HT and 5 wt% silica particle in chloroform at a concentration of 5 mg/ml. The P3HT and silica particle solution was stirred at 550 rpm at 60 °C for 1 h, followed by cooling for 1 h at room temperature. A mixture of P3HT and silica particle was then spin-coated onto the HMDS-treated substrate at 2500 rpm for 1 min to form an active layer.

Source and drain gold electrodes were deposited onto the active layer via thermal evaporation. A shadow mask was used to form a channel with a length of 100 μm and a width of 2000 μm. The deposited source and drain electrodes were connected to a sensor platform using silver paste and silver wire, respectively, to fabricate the OFET based gas sensor.

2.3. Characterization of organic gas sensor

The thickness and molecular order of the P3HT–silica blended films behavior were examined using a UV–Vis spectrophotometer (Lambda 365, PerkinElmer). The surface morphologies of the blended films were analyzed using optical microscopy (OM, BX51) and field-emission scanning electron microscopy (SEM, JSM-7800F). Charge transport characteristics of the OFET devices were measured under vacuum at room temperature (average temperature: 21.5 °C) using a probe station equipped with a Keithley 4200-SCS semiconductor parameter analyzer. The drain current was measured as a function of gate voltage (V_G) at a fixed drain voltage (V_D) of −60 V. The gas sensing characteristics were assessed at ambient temperature (average temperature: 21.8 °C), while both the gate and drain voltages were maintained at −20 V using a precision gas analysis system (GASENTEST). A certified calibration gas cylinder with nitrogen as the balance gas was employed for the measurements. The dynamic sensing responses toward NO_2, SO_2, and CO_2 were examined by adjusting the gas concentrations from 10 to 100 ppm under controlled humidity conditions (relative humidity between 20% and 40%), with a constant drain voltage of −20 V applied throughout the tests.

To evaluate the air stability of the OFET under ambient conditions, the P3HT and silica blended films were exposed to ambient atmosphere for 42 days, and the transfer curves were measured to analyze the change of drain current (I_D) with a change in gate voltage from −60 V to 60 V under fixed drain voltage at −60 V.

2.4. Sensor performance parameters

The responsivity (R) of the gas sensor was calculated using the formula $R = \Delta I_D/I_{D0}$, where I_D is the drain current measured during gas exposure, and I_{D0} is the baseline current under ambient air. The response and recovery rates, expressed as $\Delta R/\Delta t$, represent how quickly the drain current rises to its peak value or returns to baseline, respectively. Sensitivity was quantified based on the relationship between gas concentration (C_t) and the corresponding sensor response, with the slope of the linear fit indicating the degree of sensitivity. Sensitivity is defined as follows:

$$S = \frac{\partial\left(\Delta I_D/I_{DO}\right)}{\partial C_{t.}}$$

The limit of detection (LOD) is a crucial parameter in gas sensor and one of the key factors for evaluating sensor performance, as it defines the lowest analyte concentration that a sensor can reliably detect. This directly reflects the sensor's sensitivity and practical applicability. Similar to responsivity and sensitivity, the LOD is essential for quantifying sensor performance. In this study, the LOD was calculated based on the root mean square (RMS) noise of the baseline signal.

The RMS noise is a statistical indicator that represents the variability of the sensor's baseline signal, while sensitivity (slope) describes the change in the sensor response as a function of gas concentration (e.g., $\Delta I/\Delta C$). In this study, the LOD was calculated using the following formula:

$$LOD = \frac{3 \times \text{RMS noise}}{\text{slope (sensitivity)}}$$

3. Results and discussion

3.1. Characterizing silica particle and blended thin film

The surface area of the silica particles was analyzed using adsorption-desorption isotherm curves measured by the BET model (Fig. S2). Generally, BET surface area data for polymers such as polyethylene, polystyrene, and polyvinyl chloride are reported to be quite low, usually under 1 m^2/g, due to chain entanglements [25]. However, BET analysis of the functionalized silica particles with SAMs revealed that the surface area decreased from approximately 10 m^2/g for the pristine and O-silica to around 3 m^2/g after SAMs modification, regardless of the type of introduced functional group. This decrease is primarily attributed to the formation of the SAM layer, which partially blocks surface pores and limits gas adsorption [26]. The reduced surface area in all SAM-treated silica suggests that the surface functionalization was successfully and uniformly achieved.

X-ray photoelectron spectroscopy (XPS) was employed to investigate the chemical composition and surface functionalization of the silica particle modified with SAMs, as shown in Fig. 1. To confirm the successful introduction of functional groups, we analyzed the core-level spectra corresponding to the O 1 s, C 1 s, N 1 s, and S 2p photoemission regions.

In the O 1 s core-level spectra, a photoemission feature centered at 533 eV was observed for O-silica, which is characteristic of hydroxyl groups on the surface [27]. The relatively strong intensity of this signal compared to the other silica particles suggests a high density of surface silanol groups, confirming the hydroxyl-rich nature of the O-silica surface (Fig. 1a). In contrast, the O 1 s core-level spectrum of the other silica particles exhibited a shift to approximately 531 eV, which can be attributed to the formation of Si–O–Si (siloxane) bonds through condensation reactions between surface hydroxyls during the silanization process [28]. The C 1 s core-level spectrum of the C-silica exhibited a more intense photoemission feature at 283.8 eV compared to the other silica particles (Fig. 1b), indicating the presence of methyl groups introduced via SAM modification [29].

In the N 1 s core-level spectrum, signals around 397.2 eV were detected exclusively for the 2 N- and 3 N-silica, corresponding to amine-related nitrogen species (Fig. 1c). The 3 N-silica exhibited the strongest N 1 s intensity, consistent with the higher amine content introduced by the tri-amine silane precursor. Finally, the S 2p core-level spectrum was observed only in the S-silica, with a spectral feature near 162 eV (Fig. 1d), confirming the incorporation of thiol groups on the silica surface. The absence of this signal in the other silica particles further validates the selective surface modification. These XPS results collectively confirm that the silica particles were successfully and selectively functionalized with hydroxyl, methyl, diamine, triamine, and thiol groups through SAM based surface engineering.

The atomic ratios of N/Si, S/Si, and C/Si were calculated from the XPS spectra to quantitatively assess the degree of surface functionalization (Table S1). The N/Si ratio of the 3 N-silica (0.238) was higher than that of the 2 N-silica (0.197), indicating a greater incorporation of amine groups. The S-silica exhibited an S/Si ratio of 0.143, confirming successful thiol modification, and the C-silica exhibited the highest C/Si ratio (0.831), reflecting effective surface methylation.

The dispersion stability in water of silica particles functionalized with functional groups is presented in Fig. 2a. Except for the C-silica, all the other silica particles exhibit good dispersion stability, maintaining a stable suspension regardless of the surface functional group. The C-silica exhibits extremely low dispersibility due to the hydrophobic nature of the hydrocarbon alkyl groups. The hydrophobicity of the alkyl chain hinders its effective interaction with water, leading to particle aggregation and phase separation. These results further confirm the successful surface modification of the silica particles with functional groups.

The thickness and molecular order of the P3HT-silica blend films

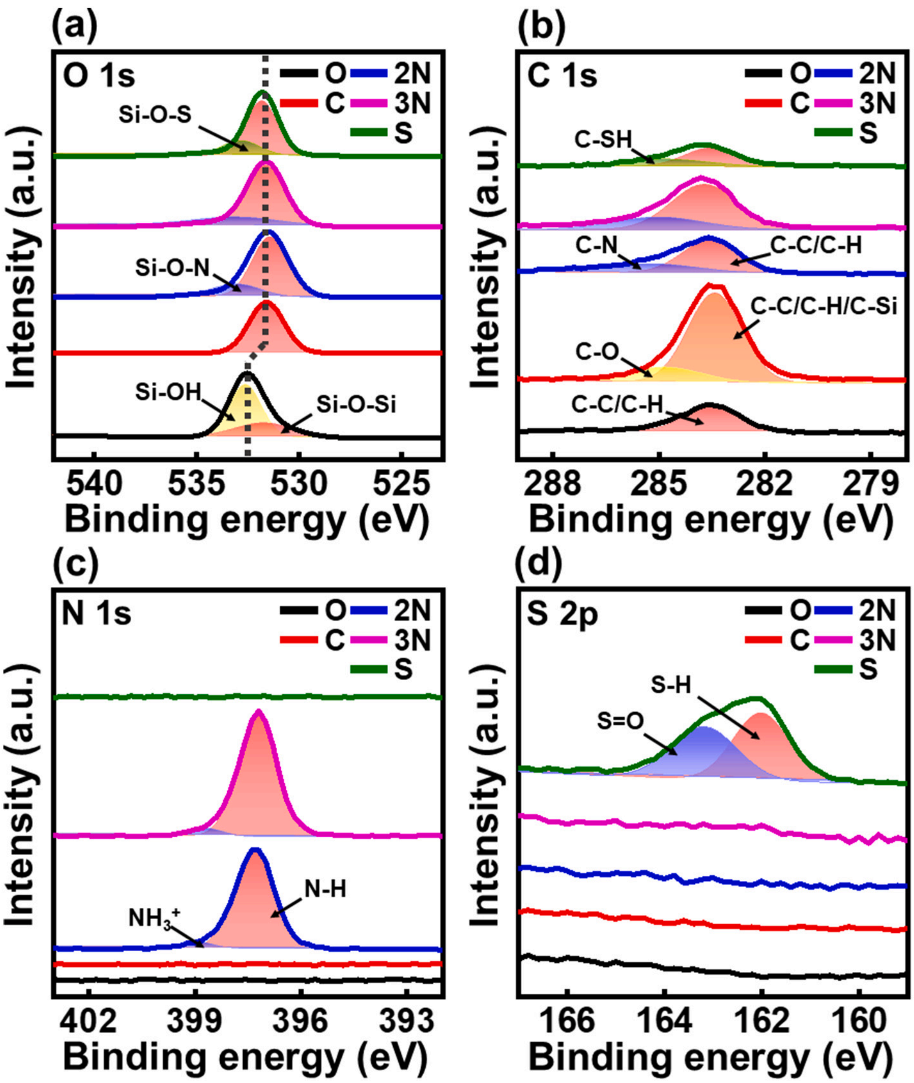

Fig. 1. XPS spectra of (a) O 1 s, (b) C 1 s, (c) N 1 s, and (d) S 2p for silica particle with functional groups.

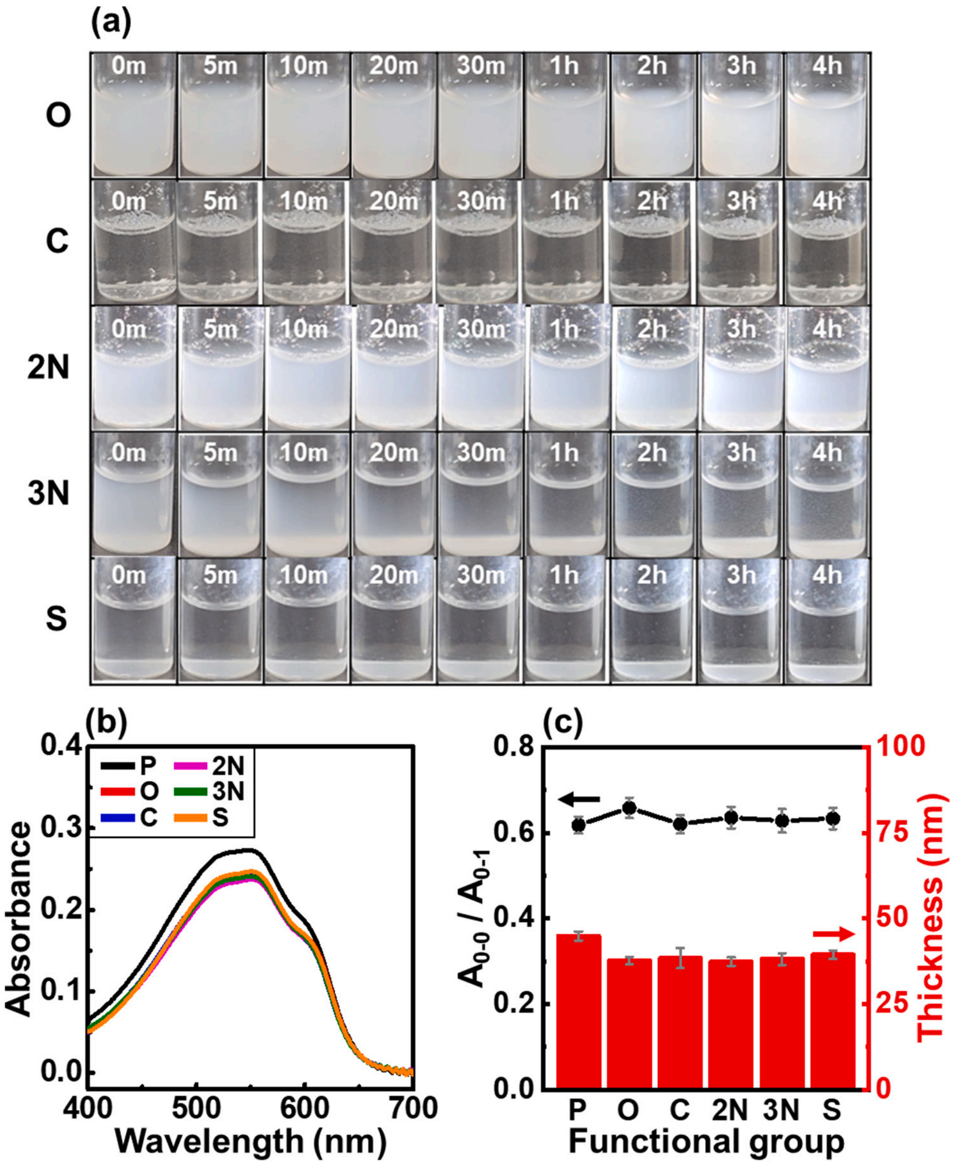

Fig. 2. (a) Photographic images showing the dispersion behavior of silica particles in deionized water over time. (b) UV-Vis absorption spectra of the P3HT film with silica particle with functional groups. (c) Molecular order of P3HT-silica blended film calculated from (0–1) peak (left axis) and the thickness of P3HT-silica blended film (right axis).

with functional group are summarized in Fig. 2b and c. Regardless of the type of the functional group on the silica particle, for all blended films weak $A_{(0-1)}$ and $A_{(0-0)}$ bands are observed at approximately 558 nm and 605 nm, respectively, which are indicative of weak P3HT chain interactions (Fig. 2b). Fig. 2c presents the variation in molecular ordering and film thickness depending on the type of functional group introduced on the silica surface. The degree of molecular order in the blended films was evaluated by comparing the intensity ratio between the $A_{(0-0)}$ and $A_{(0-1)}$ absorption peaks. Film thickness was estimated based on optical absorbance data using the Beer–Lambert law [30]. The thickness of all blended films is uniform at approximately 40 nm regardless of the type of functional group on the silica particle, and the molecular order shows no significant variation, remaining largely consistent.

The surface morphologies of the P3HT thin films blended with the surface-functionalized silica particle were analyzed using OM and SEM (Fig. S3). OM analysis revealed that all blended films exhibit uniformly distributed silica particles. SEM images further confirmed that the silica particles are uniformly dispersed within the P3HT matrix, forming particle aggregates of approximately 5 μm. These results suggest that the silica particles are well distributed within the P3HT matrix, increasing the number of gas adsorption sites in the composite film.

3.2. *Gas sensing performance of silica blended thin films*

To evaluate the charge transport characteristics of P3HT films blended with silica particles, top-contact bottom-gate transistors were fabricated on SiO_2 substrates treated with HMDS (Fig. 3). The drain current in the transfer curves was recorded as a function of gate voltage (V_G), while the drain voltage (V_D) was kept constant at −60 V. Transfer characteristics were analyzed according to the surface functional groups of the silica particles (Fig. 3a–c). Compared to homo P3HT, the incorporation of silica resulted in a notable decrease in field-effect mobility. Specifically, while the field-effect mobility of the homo P3HT device was 1.16×10^{-3} cm^2/V·s, the 3 N-silica composite film exhibited the lowest field-effect mobility value of 5.09×10^{-4} cm^2/V·s.

This reduction is primarily due to the presence of insulating silica particles that hinder charge carrier transport within the channel region. Notably, the field-effect mobility of P3HT films blended with 3 N- and S-

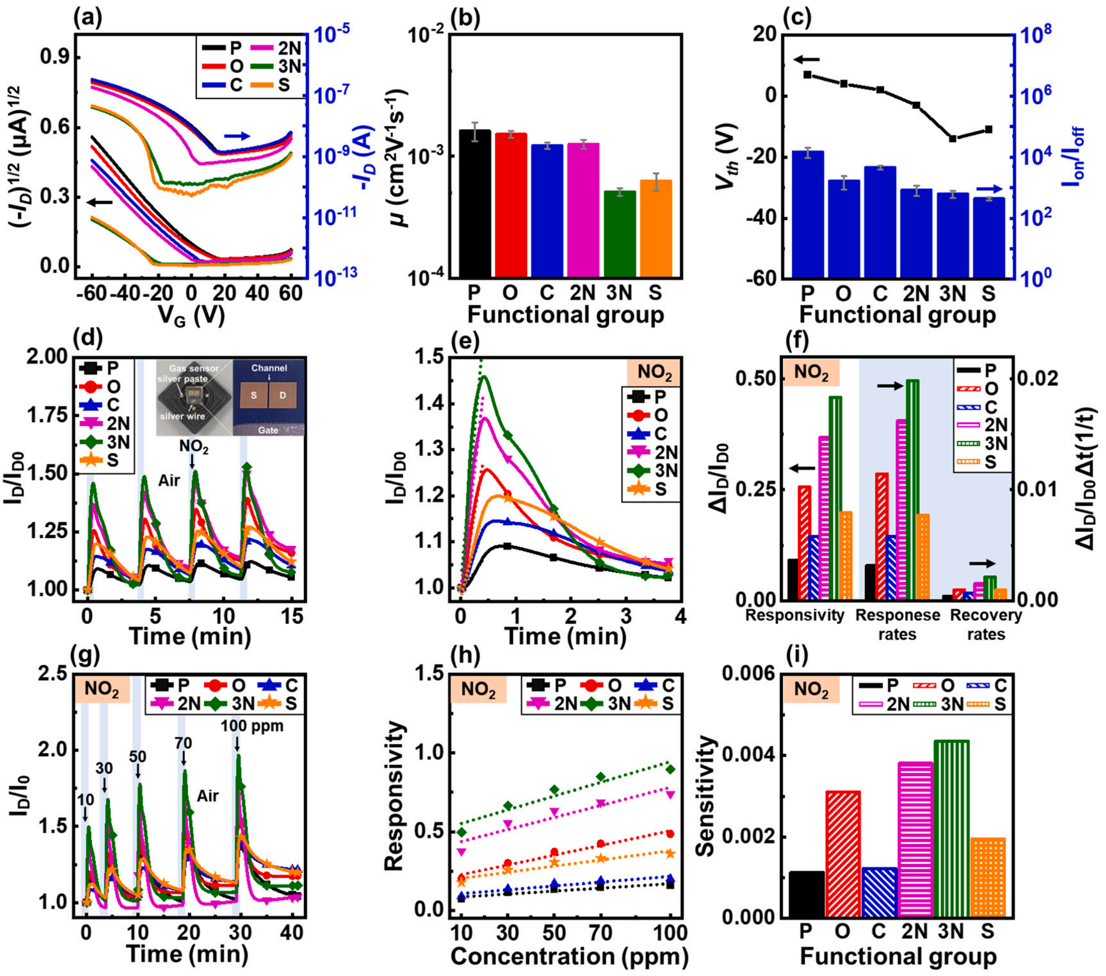

Fig. 3. (a) Transfer curve (I_D vs V_G) of OFETs at a fixed drain voltage of −60 V. (b) Field-effect mobility, (c) the threshold voltage (V_{th}) (left axis) and I_{on}/I_{off} ratio (right axis) of P3HT-silica blended films with functional groups. (d) Repeated gas detection curve and (inset) optical photograph of the organic gas sensor and (e) magnified first gas detection cycle curve under 10 ppm NO₂ exposure. (f) Summary of sensing performance under repeated NO₂ injection (10 ppm). (g) Dynamic gas sensing performance of P3HT-silica blended thin film exposed to various concentrations of NO$_2$ (10–100 ppm). (h) Linear fit showing the responsivity of organic gas sensor following introduction of 10 ppm NO₂. (i) Sensitivity of organic gas sensor calculated from the slope of the linear fitted graphs.

silica significantly decreased, and the threshold voltage (V_{th}) shifted toward more negative values in the transfer curves. These effects are attributed to the electron-donating nature of the amine and thiol functional groups, which reduce hole carrier density in the p-type channel, resulting in a lower current level compared to the pristine P3HT device [31]. The lower hole concentration also leads to the formation of the conductive channel at higher gate voltages, thereby shifting the threshold voltage shifts toward negative value.

Moreover, the introduction of strong dipolar groups, such as 3 N and S–silica, is known to induce charge trapping or scattering centers at the dielectric/semiconductor interface. These interfacial dipoles disrupt the local electrostatic environment, further impeding charge transport and contributing to a shift in threshold voltage, consistent with the observed behavior in the 3 N- and S-silica [32].

We investigated the gas-sensing capacity of P3HT blended films with functional groups on the silica particle. The gas sensing performance was measured by observing the drain current ($I_D(t)/I_D(0)$) with both V_D and V_G fixed at −20 V (Fig. 3d–f). Previous studies have demonstrated that lower gate voltages enhance responsivity by allowing greater modulation of the source-drain current upon gas exposure because of reduced initial carrier concentration. In comparison, when a higher gate voltage is applied, the carrier density in the channel becomes sufficiently large and reaches saturation, which reduces the degree to which gas adsorption can influence the electrical response. Although $V_G = -10$ V exhibits the highest responsivity in some reports, variations in charge carrier density due to surface characteristics can significantly affect reproducibility. Therefore, $V_G = -20$ V was selected to achieve a stable sensing response while maintaining high sensitivity.

The detection response was recorded again by introducing 10 ppm of NO₂ to the organic gas sensor for 20 s, followed by 500 s purge with air. The P3HT gas sensor blended with silica particle exhibited changes in current upon exposure to NO$_2$ gas, and the current was recovered when air was introduced. Due to the strong electron-withdrawing nature of NO$_2$, exposure to the gas resulted in charge carrier accumulation in the channel region, leading to an increase in the current level ($I_D(t)/I_D(0)$) [33]. The gas sensors based on P3HT blended with silica particle exhibited higher drain current values than the homo P3HT sensors. The gas sensing performance, based on the type of functional groups, improved in the order of C, S, O, 2 N, and 3 N. Notably, the sensors blended with silica containing amine functional groups exhibited a significant increase in drain current, resulting in high responsivity ($R = \Delta I_D/I_{D0}$) and response rates ($\Delta R/\Delta t$). Among the various functional groups, the gas sensor blended with 3 N-silica showed the highest responsivity of 0.459 for 10 ppm NO$_2$ gas, which is more than five times greater than that of the homo P3HT sensor. This enhancement is attributed to the difference in reactivity between the silica functional groups and gas molecules [34–36]. The strong reactivity between NO$_2$ and the amine functional groups led to a significantly improved gas sensing performance compared to the homo P3HT sensor or other functional groups [37,38].

The response rate was determined from the slope of the I_D/I_{D0} curve following NO_2 injection, while the recovery rate was calculated from the falling slope after air purging. Among all the silica particles, the sensor blended with 3 N-silica exhibited the fastest response and recovery rates, indicating efficient NO_2 adsorption and desorption kinetics due to the strong interaction between the amine group and NO_2. Considering responsivity, response rate, and recovery rate together, the sensor blended with 3 N-silica clearly outperformed the sensor blended with other functionalized silica.

The dynamic gas sensing performance is analyzed in Fig. 3g–i for NO_2 concentrations varying from 10 to 100 ppm. The dynamic gas sensing performance of the P3HT sensors blended with silica particle were measured by observing the changes in the drain current during repeated exposure to NO_2 gas for 20 s, followed by air purging. As observed in the repeated detection test with 10 ppm NO_2, the gas sensors blended with silica particle exhibit enhanced gas sensing performance compared to those of the homo P3HT sensors. The sensitivity of the gas sensors was calculated based on the slope of the response as a function of increasing NO_2 concentration. Among the various functional groups, the sensor blended with 3 N-silica exhibited a sensitivity of approximately 0.00436, which is approximately four times higher than the sensitivity of 0.00112 observed in the homo P3HT gas sensor.

According to previous studies, gas sensing properties were enhanced by analyzing the differences in intermolecular binding energies between functional groups and gas molecules. Using quantum mechanical calculations and density functional theory, the binding energies between the various functional groups and NO_2 gas molecules were computed [22,39,40]. Among the functional groups, the amine groups exhibited the highest binding energy, more than twice as large as that of the methyl group. This indicates that NO_2 molecules bind strongly to the amine functional group [38]. When the gas molecules react with the functional groups on the silica surface, the adsorbed NO_2 molecules act as electron acceptors, leading to a p-type doping effect, which increases the drain current. In contrast, C-silica showed relatively weaker chemical bonding with NO_2, resulting in less pronounced sensor responsiveness. In contrast, the hydroxyl and amine groups showed high reactivity with NO_2 gas molecules, such that when NO_2 is adsorbed onto the surface, it acts as an electron acceptor, increasing the hole carrier density. As P3HT is a p-type semiconductor, the capture of electrons by NO_2 increases the hole carrier density, leading to an increase in the drain

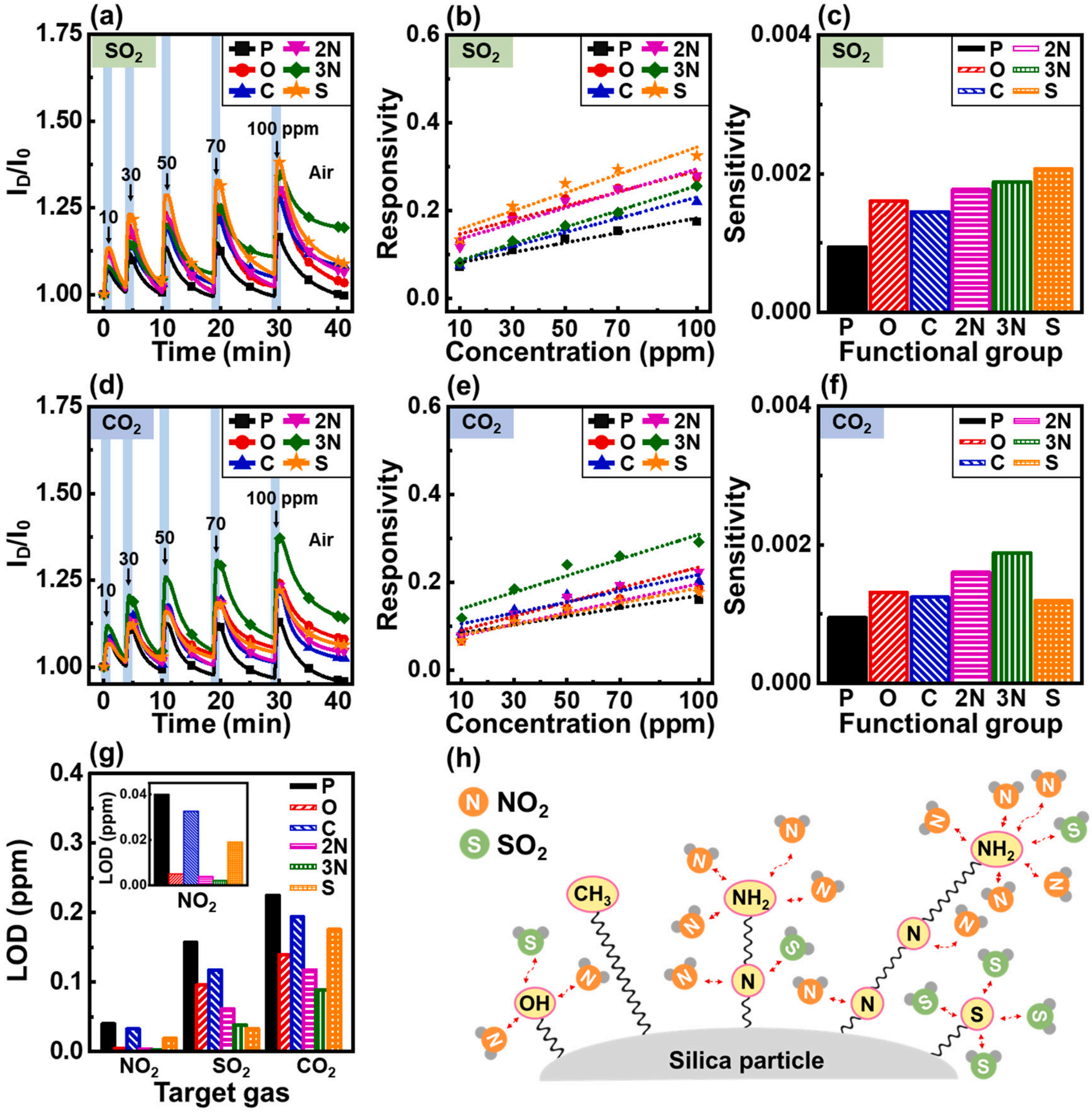

Fig. 4. Summary of dynamic gas sensing performance at various concentration of SO_2: (a) dynamic sensing curve, (b) responsivity, and (c) sensitivity. Summary of dynamic gas sensing performance at various concentration of CO_2: (d) dynamic sensing curve, (e) responsivity, and (f) sensitivity. (g) Calculated LOD of various target gases (NO_2, SO_2, CO_2). (e) Schematic illustration of interaction between harmful gases and the functional group of surface modified silica particles.

current and high responsiveness of the OFET based gas sensor.

To evaluate the selectivity of the gas sensors, dynamic responses to SO_2 and CO_2 were measured under conditions identical to those used in the NO_2 sensing tests (Fig. 4). Analysis of the dynamic gas detection properties of SO_2 and CO_2 showed significantly lower current changes than those of NO_2. SO_2 and CO_2 exhibit lower reactivity and sensitivity than NO_2, possibly because of the differences in the oxidation ability of the gas molecules [41]. NO_2, a strong oxidizer, can easily extract electrons, resulting in higher reactivity and sensitivity in gas sensor devices. In contrast, CO_2 is a non-polar and symmetric molecule with low reactivity and sensitivity.

Among the functional groups, the S-silica exhibited the highest sensitivity and best gas detection performance for SO_2. This is due to the strong chemical interaction between SO_2 and the sulfur atom in the thiol group. SO_2 is an acidic oxide that can react with thiol groups to form stable sulfur-containing complexes, leading to significant changes in the electrical properties of the organic gas sensor. The thiol group can chemically bind to SO_2 molecules, which results in more pronounced shifts in the threshold voltage and drain current, indicating efficient gas sensing. The other functional groups exhibited weaker interactions, with SO_2, leading to lower gas sensitivity.

CO_2 gas sensing performance exhibited a trend similar to that of NO_2. CO_2 molecules can react with amine groups to form stable carbamate complexes, enhancing the gas sensing efficiency. This chemical interaction between CO_2 and the amine groups enables strong binding and results in a significant change in the electrical characteristics of the organic gas sensor. The hydroxyl groups also showed moderate sensitivity to CO_2 due to hydrogen bonding although their performance was not as strong as that of the amine-functionalized silica. The methyl groups, being hydrophobic, showed minimal interaction with CO_2, resulting in poor gas detection.

In order to assess the sensing capability for different harmful gases, including NO_2, SO_2, and CO_2, LOD was estimated based on established methodologies reported in prior studies [42]. For all functional groups, lower LOD values were observed for NO_2 than for SO_2 and CO_2 gases. For NO_2 gas, 3 N-silica exhibited the lowest detection limit of 0.00208 ppm. For SO_2, S-silica showed the lowest detection limit of 0.0332 ppm, and for CO_2, 3 N-silica exhibited the lowest detection limit of 0.0892 ppm. These findings suggest that gas sensors incorporating P3HT and silica particle exhibit strong selectivity toward NO_2 molecules.

Based on these results, we compared the overall sensing performance with previously reported OFET based gas sensors. The calculated LOD is summarized in Table S2 [43–47]. These results clearly indicate that surface-functionalized silica significantly enhances gas sensing performance by improving the sensitivity and lowering the detection limit. Furthermore, this study demonstrates a simple and versatile approach for selectively tuning gas sensing behavior through the surface modification of silica with SAMs.

3.3. *Air stability*

A significant drawback of organic gas sensors is their poor air stability, which is primarily caused by oxidative degradation of the organic active layer [48,49]. This degradation can lead to a shift in the threshold voltage or an increase in the off-current, adversely affecting device performance. To evaluate how the organic transistors perform after extended exposure to air, their transfer characteristics were measured following 42 days of storage under room temperature ambient conditions (Fig. 5). The OFETs were characterized in three states: freshly prepared, after 42 days of ambient storage, and after recovery under vacuum conditions. The p-type OFET exhibited a positive shift in the threshold voltage (V_{th}), which was attributed to the adsorption of water and oxygen (Fig. 5g). These molecules introduce negative charges that are trapped at the interface and within the grain boundaries, leading to instability.

After storage in ambient conditions (average temperature: 20 ± 2 °C, relative humidity: ~30 ± 10%), a significant degradation in device performance was observed across all OFETs. This behavior can be attributed to moisture and oxygen uptake, leading to the formation of traps at the interface and within the semiconductor layer [50]. As a result of this charge trapping, the hole density in the semiconductor layer decreased, causing an increase in the off-current and a shift in V_{th} to the right (Figs. 5a–f). The trapped charges hinder charge carrier transport, further increasing the off-current, thereby degrading the overall device performance [51,52]. Notably, O- and N-silica exhibited a significant increase in off-current due to the higher adsorption of H_2O from the ambient environment [53].

Upon vacuum treatment, a partial recovery of the device performance was observed in some silica particles. In the thin films blended with surface-functionalized silica, the recovery rate improved by approximately 5–8 times compared to that of the homo P3HT film. This recovery is due to the removal of physically adsorbed moisture and oxygen. In particular, O-, 2 N-, 3 N-, and S-silica facilitate reversible interactions with oxygen and water in the atmosphere, enabling the

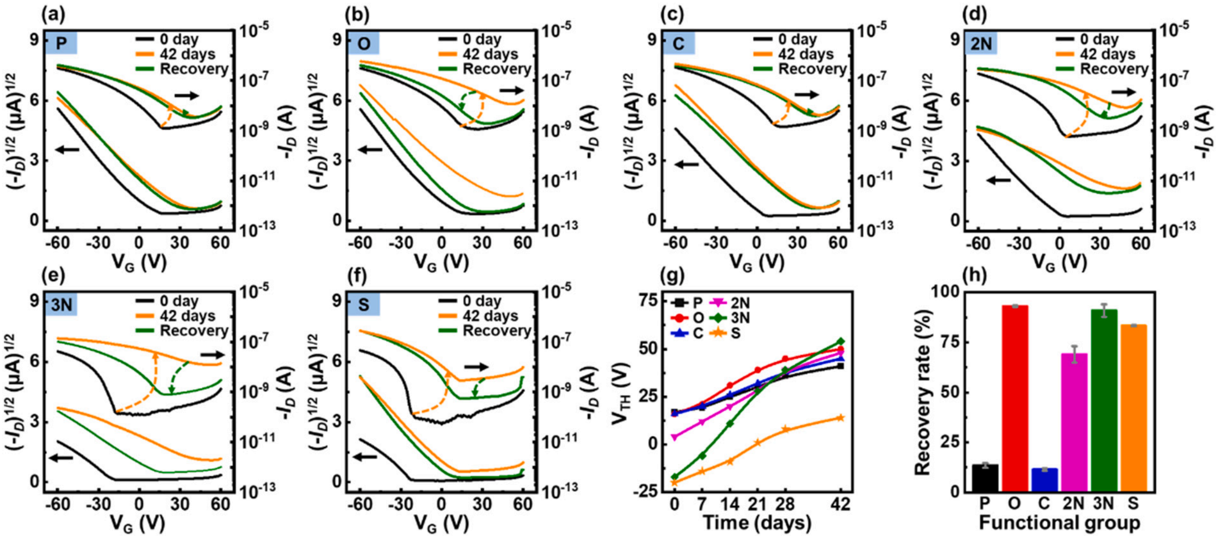

Fig. 5. Transfer curve of the OFETs: (a) homo P3HT; and P3HT blended with (b) O, (c) C, (d) 2 N, (e) 3 N, and (f) S-silica. Summary of air stability test; (g) V_{th} shift and (h) recovery rate of OFET.

recovery of electrical properties upon vacuum treatment [54]. The chemical modification of silica surfaces effectively protects the conjugated polymer film from charge trapping and oxidative reactions, contributing to the long-term stability of OFET devices.

To evaluate the air stability of the OFET device quantitatively, the recovery rate of I_{off} was calculated using the following equation:

$$Recovery\ rate(I_{off}) = \frac{(I_{off})_{recovery} - (I_{off})_{42day}}{(I_{off})_{0day} - (I_{off})_{42day}} \times 100\%$$

P3HT and C-silica exhibited low recovery rates of approximately 10%, whereas 2 N- and S-silica exhibited higher recovery rates of 70% and 80%, respectively. Notably, 3 N- and O-silica achieved the highest recovery rate of 90%. These results indicate that surface-functionalized silica not only enhances the gas adsorption properties but also significantly improves the air stability of OFET devices.

Air stability of gas sensor was investigated over 14 days (Fig. S4). The sensor blended with 3 N-silica, which exhibited the highest NO_2 sensing performance, was compared directly with the homo P3HT sensor. Both sensors showed a reduction in sensing performance; however, the sensor with 3 N-silica showed less reduction in sensing performance. The sensitivity of the sensor with 3 N-silica remained above 80% of its initial value, indicating enhanced long-term stability. The amine groups inhibit oxidative decomposition induced by ambient oxygen or moisture through their weak basicity. Additionally, the functionalized silica nanoparticles may act as a protective barrier, limiting the diffusion of reactive species into the conjugated polymer layer. It is well known that moisture exposure can lead to oxidation of the conjugated polymer and the formation of deep trap states, which reduce drain current and sensing performance. In particular, 3 N-silica showed a strong interaction with NO_2 under atmosphere condition.

Furthermore, additional sensing performance change under different relative humidity (RH) conditions (RH 20%, 40%, and 60%) was measured (Fig. S4c–f). As the humidity level increased, both sensors exhibited a gradual decline in sensitivity due to the competitive adsorption of water molecules, which interferes with the adsorption of NO_2. However, the sensor with 3 N-silica consistently showed a smaller decrease in sensing performance compared to the homoP3HT sensor. This improvement is due to the amine groups' ability to interact with NO_2 under humid conditions. These results demonstrated that the sensor with 3 N-silica exhibits high gas sensing performance and superior stability [54,55].

4. Conclusion

In this study, we investigate the effects of surface-modified silica particles on the performance of organic gas sensors. The incorporation of functionalized silica significantly influenced the charge transport characteristics and gas adsorption properties. Among the various functional groups, amine functionalized silica exhibited the highest gas sensing performance, particularly for NO_2 detection due to their strong binding affinity with gas molecules. Conversely, for SO_2 detection, S-silica demonstrated superior sensing performance, attributed to the strong chemical affinity between SO_2 and thiol groups. These findings indicate that tuning the surface functional groups of silica enables precise control over gas-surface interactions, thereby selectively enhancing the gas adsorption properties. Although the SAM based surface modification reduces the surface area of silica particles, it enhances the reactivity between the surface functional groups and gas molecules, thereby improving the gas sensing performance when incorporated into the sensing layer. Furthermore, air stability tests demonstrated that the functionalized silica improved the operational stability of OFET devices, with 3 N- and O-silica achieving the highest recovery rates. These results confirm that the surface engineering of silica particles is an effective strategy for improving the sensitivity, selectivity, and long-term stability of organic gas sensors, making them highly promising for practical applications in environmental monitoring and industrial safety. In addition to improvements in sensing performance and stability, this approach also provides practical advantages in terms of process simplicity and commercial viability. Our method avoids structurally complex ligand exchange processes and the use of expensive porous materials, thereby providing a cost-effective route to enhance gas sensing performance.

CRediT authorship contribution statement

In Hwa Ko: Writing – original draft, Investigation, Formal analysis, Data curation. **So Jeong Park:** Investigation, Formal analysis, Data curation. **Yeong Don Park:** Writing – review & editing, Supervision, Funding acquisition, Conceptualization.

Declaration of competing interest

The authors declare that they have no known competing financial interests or personal relationships that could have appeared to influence the work reported in this paper.

Acknowledgments

This work was supported by the National Research Foundation of Korea (NRF) grant funded by the Korea government (MSIT) (No. NRF2023R1A2C1005218).

Appendix A. Supplementary data

Supplementary data to this article can be found online at https://doi.org/10.1016/j.cej.2025.165032.

Data availability

Data will be made available on request.

References

[1] B.F. Bessac, S.-E. Jordt, Sensory detection and responses to toxic gases: mechanisms, health effects, and countermeasures, Proc. Am. Thorac. Soc. 7 (4) (2010) 269–277.

[2] J.O. Anderson, J.G. Thundiyil, A. Stolbach, Clearing the air: a review of the effects of particulate matter air pollution on human health, J. Med. Toxicol. 8 (2012) 166–175.

[3] T. Boningari, P.G. Smirniotis, Impact of nitrogen oxides on the environment and human health: Mn−based materials for the NO_x abatement, Curr. Opin. Chem. Eng. 13 (2016) 133–141.

[4] V. Chaudhary, N. Ashraf, M. Khalid, R. Walvekar, Y. Yang, A. Kaushik, Y.K. Mishra, Emergence of MXene–polymer hybrid nanocomposites as high-performance next-generation chemiresistors for efficient air quality monitoring, Adv. Funct. Mater. 32 (33) (2022) 2112913.

[5] S.M. Horvath, Nitrogen dioxide, pulmonary function, and respiratory disease, Bull. N. Y. Acad. Med. 56 (9) (1980) 835.

[6] C. Zhang, Y. Luo, J. Xu, M. Debliquy, Room temperature conductive type metal oxide semiconductor gas sensors for NO_2 detection, Sens. Actuators, A 289 (2019) 118–133.

[7] S. Hong, M. Wu, Y. Hong, Y. Jeong, G. Jung, W. Shin, J. Park, D. Kim, D. Jang, J.-H. Lee, FET−type gas sensors: a review, Sensors Actuators B Chem. 330 (2021) 129240.

[8] Y. Wang, J. Zhang, S. Zhang, J. Huang, OFET chemical sensors: chemical sensors based on ultrathin organic field-effect transistors, Polym. Int. 70 (4) (2021) 414–425.

[9] C. He, J. Cheng, X. Zhang, M. Douthwaite, S. Pattisson, Z. Hao, Recent advances in the catalytic oxidation of volatile organic compounds: a review based on pollutant sorts and sources, Chem. Rev. 119 (7) (2019) 4471–4568.

[10] S.G. Surya, H.N. Raval, R. Ahmad, P. Sonar, K.N. Salama, V.R. Rao, Organic field effect transistors (OFETs) in environmental sensing and health monitoring: a review, TrAC Trends Anal. Chem. 111 (2019) 27–36.

[11] S. Pavithra, R. Thejas, H.A. Rao, B. Krishna, G. Nagaraju, Preparation of polypyrrole by chemical oxidation: applications for sensor studies, Macromol. Res. 32 (1) (2024) 23–33.

[12] J. Hwang, J. Shin, W.H. Lee, Recent achievements in conjugated polymer−based gas sensors by side−chain engineering, Macromol. Res. 33 (2024) 1–14.

[13] I.H. Ko, S.Y. Park, Y.D. Park, Controlling the molecular weight of poly (3−hexylthiophene) for highly sensitive and flexible gas sensor, Sensors Actuators B Chem. 7 (5) (2025) 137554.

[14] H. Chen, S. Dong, M. Bai, N. Cheng, H. Wang, M. Li, H. Du, S. Hu, Y. Yang, T. Yang, Solution-processable, low-voltage, and high-performance monolayer field-effect transistors with aqueous stability and high sensitivity, Adv. Mater. 27 (12) (2015) 2113–2120.

[15] B. Kang, M. Jang, Y. Chung, H. Kim, S.K. Kwak, J.H. Oh, K. Cho, Enhancing 2D growth of organic semiconductor thin films with macroporous structures via a small−molecule heterointerface, Nat. Commun. 5 (1) (2014) 4752.

[16] B. Nketia−Yawson, A.−.R. Jung, Y. Noh, G.−.S. Ryu, G.D. Tabi, K.−.K. Lee, B. Kim, Y.−.Y. Noh, Highly sensitive flexible NH_3 sensors based on printed organic transistors with fluorinated conjugated polymers, ACS Appl. Mater. Interfaces 9 (8) (2017) 7322–7330.

[17] H.J. Cheon, S.Y. Shin, V. Van Tran, B. Park, H. Yoon, M. Chang, Preparation of conjugated polymer/reduced graphene oxide nanocomposites for high−performance volatile organic compound sensors, Chem. Eng. J. 425 (2021) 131424.

[18] S. Mallik, S. Chand Pal, S. Acharyya, S.P. Verma, A. Mandal, P.K. Guha, M.C. Das, D.K. Goswami, MOF−assimilated high−sensitive organic field−effect transistors for rapid detection of a chemical warfare agent, ACS Appl. Mater. Interfaces 15 (25) (2023) 30580–30590.

[19] C. Haensch, S. Hoeppener, U.S. Schubert, Chemical modification of self−assembled silane based monolayers by surface reactions, Chem. Soc. Rev. 39 (6) (2010) 2323–2334.

[20] S.P. Pujari, L. Scheres, A.T. Marcelis, H. Zuilhof, Covalent surface modification of oxide surfaces, Angew. Chem. Int. Ed. 53 (25) (2014) 6322–6356.

[21] A. Keshavaraja, B. Jayashri, A. Ramaswamy, K. Vijayamohanan, Effect of surface modification due to superacid species in controlling the sensitivity and selectivity of SnO_2 gas sensors, Sensors Actuators B Chem. 23 (1) (1995) 75–81.

[22] Y.E. Hahm, B.H. Park, S.Y. Park, T.K. An, J. Lee, Y.D. Park, Enhancement of NO_2 gas sensing ability through strong binding energy by modification of interface characteristics, Org. Electron. 104 (2022) 106493.

[23] F. Ali, C. Roldán-Carmona, M. Sohail, M.K. Nazeeruddin, Applications of self-assembled monolayers for perovskite solar cells interface engineering to address efficiency and stability, Adv. Energy Mater. 10 (48) (2020) 2002989.

[24] M. Hong, W. Jo, S.A. Jo, H. Jin, M. Kim, C.Y. Lee, Y.D. Park, Enhanced gas sensing characteristics of a polythiophene gas sensor blended with UiO-66 via ligand functionalization, Adv. Electron. Mater. 10 (8) (2024) 2300901.

[25] K.N. Fotopoulou, H.K. Karapanagioti, Surface properties of beached plastic pellets, Mar. Environ. Res. 81 (2012) 70–77.

[26] Z. Li, X. Yan, K. Wu, Y. Jiao, C. Zhou, J. Yang, Surface modification of reduced graphene oxide beads: integrating efficient endotoxin adsorption and improved blood compatibility, ACS Appl. Bio Mater. 4 (6) (2021) 4896–4906.

[27] V. Antunes, C. Figueroa, F. Alvarez, A comprehensive study of the TiN/Si interface by X−ray photoelectron spectroscopy, Appl. Surf. Sci. 448 (2018) 502–509.

[28] A. Hashemi, A. Bahari, Structural and dielectric characteristic of povidone–silica nanocomposite films on the Si (n) substrate, Appl. Phys. A Mater. Sci. Process. 123 (2017) 1–7.

[29] M.Y. Bashouti, Y. Paska, S.R. Puniredd, T. Stelzner, S. Christiansen, H. Haick, Silicon nanowires terminated with methyl functionalities exhibit stronger Si–C bonds than equivalent 2D surfaces, Phys. Chem. Chem. Phys. 11 (20) (2009) 3845–3848.

[30] D.F. Swinehart, The beer−lambert law, J. Chem. Educ. 39 (7) (1962) 333.

[31] B. Ronnasi, B. King, S. Brixi, S. Swaraj, J. Niskanen, B.H. Lessard, Electron donating functional polymer dielectrics to reduce the threshold voltage of n-type organic thin-film transistors, Adv. Electron. Mater. 10 (8) (2024) 2300810.

[32] J. Veres, S. Ogier, G. Lloyd, D. De Leeuw, Gate insulators in organic field−effect transistors, Chem. Mater. 16 (23) (2004) 4543–4555.

[33] C. Tanase, P. Blom, D. De Leeuw, E. Meijer, Charge carrier density dependence of the hole mobility in poly (p-phenylene vinylene), Phys. Status Solidi A 201 (6) (2004) 1236–1245.

[34] C. Zhang, P. Chen, W. Hu, Organic field−effect transistor−based gas sensors, Chem. Soc. Rev. 44 (8) (2015) 2087–2107.

[35] X. Wang, X. Li, Y. Zhao, Y. Chen, J. Yu, J. Wang, The influence of oxygen functional groups on gas−sensing properties of reduced graphene oxide (rGO) at room temperature, RSC Adv. 6 (57) (2016) 52339–52346.

[36] J. Wagner, H.−.J. Jang, J. Han, H.E. Katz, Enhanced and unconventional responses in chemiresistive sensing devices for nitrogen dioxide and ammonia from carboxylated alkylthiophene polymers, Mater. Horiz. 7 (5) (2020) 1358–1371.

[37] J. Wagner, Y. Song, J. Shapiro, H.E. Katz, Oxygen−bearing functionalities enhancing NO_2, NH_3, and acetone electronic response and response variation by polythiophenes in organic field−effect transistor sensors, J. Mater. Chem. C 10 (6) (2022) 2149–2162.

[38] S.J. Park, J.Y. Kim, D.H. Kim, D. Jang, Y.D. Park, Additive engineering for high−performance polythiophene gas sensors incorporating functional amine additive with strong binding energy for NO_2, J. Mater. Chem. C 12 (27) (2024).

[39] D. Raptis, C. Livas, G. Stavroglou, R.M. Giappa, E. Tylianakis, T. Stergiannakos, G. E. Froudakis, Surface modification strategy for enhanced NO_2 capture in metal–organic frameworks, Molecules 27 (11) (2022) 3448.

[40] L. Benoit, Interactions of NO_2 with Amine−Functionalized SBA−15: Effects of Synthesis Route, 2012.

[41] M. Hong, S.Y. Park, J.E. Lee, Y.D. Park, High−performance flexible organic gas sensor via alkyl side chain engineering of polyalkylthiophene, Chem. Eng. J. 480 (2024) 147962.

[42] Y. Qin, X. Wang, J. Zang, Ultrasensitive ethanol sensor based on nano−Ag&ZIF−8 co−modified SiNWs with enhanced moisture resistance, Sensors Actuators B Chem. 340 (2021) 129959.

[43] J. Liang, Z. Song, S. Wang, X. Zhao, Y. Tong, H. Ren, S. Guo, Q. Tang, Y. Liu, Cobweb−like, ultrathin porous polymer films for ultrasensitive NO_2 detection, ACS Appl. Mater. Interfaces 12 (47) (2020) 52992–53002.

[44] Y. Ahn, Y. Kang, H. Kye, M.S. Kim, W.H. Lee, B.−.G. Kim, Exploring pore formation and gas sensing kinetics using conjugated polymer–small molecule blends, ACS Appl. Mater. Interfaces 16 (24) (2024) 31719–31728.

[45] G. Jeong, H.J. Cheon, S.Y. Shin, E. Wi, P. Kyokunzire, H. Cheon, V. Van Tran, T. T. Vu, M. Chang, Improved NO_2 gas sensing performance of nanoporous conjugated polymer (CP) thin films by incorporating preformed CP nanowires, Dyes Pigments 214 (2023) 111235.

[46] L. Wang, L. Wang, G. Li, Y. Zhu, C. Liu, L. Zeng, S. Zhong, L.J. Wang, Three−dimensional CuPc films decorated with well−ordered PVA parallel nanofiber arrays for low concentration detecting NO_2 sensor, Sensors Actuators B Chem. 337 (2021) 129781.

[47] H. Chae, J.M. Han, Y. Ahn, J.E. Kwon, W.H. Lee, B.G. Kim, NO_2-affinitive amorphous conjugated polymer for field-effect transistor sensor toward improved NO_2 detection capability, Adv. Mater. Technol. 6 (11) (2021) 2100580.

[48] T. Kubo, R. Häusermann, J. Tsurumi, J. Soeda, Y. Okada, Y. Yamashita, N. Akamatsu, A. Shishido, C. Mitsui, T. Okamoto, Suppressing molecular vibrations in organic semiconductors by inducing strain, Nat. Commun. 7 (1) (2016) 11156.

[49] X. Chen, Z. Wang, J. Qi, Y. Hu, Y. Huang, S. Sun, Y. Sun, W. Gong, L. Luo, L. Zhang, Balancing the film strain of organic semiconductors for ultrastable organic transistors with a five−year lifetime, Nat. Commun. 13 (1) (2022) 1480.

[50] G. Chen, Z. Xu, Charge trapping and detrapping in polymeric materials, J. Appl. Phys. 106 (12) (2009).

[51] Z. Yang, C. Guo, C. Shi, D.−.K. Wang, T. Zhang, Q. Zhu, Z.−.H. Lu, Improving bias−stress stability of p−type organic field−effect transistors by constructing an electron injection barrier at the drain electrode/semiconductor interfaces, ACS Appl. Mater. Interfaces 12 (37) (2020) 41886–41895.

[52] X. Wu, R. Jia, J. Pan, J. Wang, W. Deng, P. Xiao, X. Zhang, J. Jie, Improving ideality of P-type organic field-effect transistors via preventing undesired minority carrier injection, Adv. Funct. Mater. 31 (19) (2021) 2100202.

[53] P.−.G. Su, Z.−.M. Lu, Flexibility and electrical and humidity−sensing properties of diamine−functionalized graphene oxide films, Sensors Actuators B Chem. 211 (2015) 157–163.

[54] M. Hong, P.U. Do, C.H. Lee, Y.D. Park, Enhanced gas sensing performance of polythiophene film with surface engineered porous carbon, Appl. Surf. Sci. 692 (2025) 162679.

[55] Q.T. Vu, H. Yamada, K. Yogo, Effects of amine structures on oxidative degradation of amine−functionalized adsorbents for CO_2 capture, Ind. Eng. Chem. Res. 60 (13) (2021) 4942–4950.